

Measuring the penetration depth anisotropy in MgB₂ using small-angle neutron scattering

D. Pal,¹ L. DeBeer-Schmitt,¹ T. Bera,¹ R. Cubitt,² C. D. Dewhurst,² J. Jun,³ N. D. Zhigadlo,³ J. Karpinski,³ V. G. Kogan,⁴ and M. R. Eskildsen^{1,*}

¹*Department of Physics, University of Notre Dame, Notre Dame, Indiana 46556, USA*

²*Institut Laue-Langevin, 6 Rue Jules Horowitz, F-38042 Grenoble, France*

³*Laboratory for Solid State Physics, ETH, CH-8093 Zürich, Switzerland*

⁴*Ames Laboratory and Department of Physics and Astronomy, Iowa State University, Ames, Iowa 50011, USA*

(Received 8 October 2005; published 26 January 2006)

Using small-angle neutron scattering, we have measured the misalignment between an applied field of 4 kOe and the flux-line lattice in MgB₂, as the field is rotated away from the *c* axis by an angle θ . The measurements, performed at 4.9 K, showed the vortices canting towards the *c* axis for all field orientations. Using a two-band/two-gap model to calculate the magnetization, we are able to fit our results yielding a penetration depth anisotropy, $\gamma_\lambda = 1.1 \pm 0.1$.

DOI: 10.1103/PhysRevB.73.012513

PACS number(s): 74.25.Qt, 74.70.Ad, 61.12.Ex, 74.20.-z

The two-band/two-gap nature of superconductivity in magnesium diboride (MgB₂) is well established.¹ In this material supercarriers reside on two distinctively different parts of the Fermi surface, with the larger energy gap ($\Delta_\sigma \approx 7$ meV) originating from σ bonding of p_{xy} boron orbitals, and the smaller gap ($\Delta_\pi = 2.2$ meV) arising from π bonding of the p_z orbitals.²⁻⁴ Furthermore, the π band is isotropic, while the σ band is nearly two dimensional.

The anisotropy of a type II superconductor is described either by $\gamma_\lambda = \lambda_c / \lambda_{ab}$, where λ is the magnetic penetration depth, or by $\gamma_H = H_{c2,ab} / H_{c2,c} = \xi_{ab} / \xi_c$, with ξ being the coherence length. Traditionally these two anisotropies have been considered to be identical, but in materials with anisotropic gaps this is generally not the case.⁵⁻⁷ Magnesium diboride represents an extreme case where $\gamma_H \neq \gamma_\lambda$. Theoretical work for this material indicates $\gamma_\lambda(0) \approx 1.1$ and $\gamma_H(0) \approx 6$ at low temperatures, merging at $\gamma_\lambda(T_c) = \gamma_H(T_c) \approx 2.6$ at the critical temperature T_c .^{5,7,8}

While there is experimental consensus on the temperature dependence of γ_H ,⁹⁻¹⁵ it has recently been suggested that superconductivity in MgB₂ can be described by a single anisotropy factor, $\gamma(H) = \gamma_\lambda(H) = \gamma_\xi(H)$, changing from $\gamma(H=0) \sim 1$ to $\gamma(H=H_{c2}) \sim 6$.^{14,16} However, measurements of $\gamma_\lambda(H)$ are still contradictory, with flux-line lattice (FLL) imaging and torque magnetometry measurements yielding results ranging from an arguably field-independent value of $\gamma_\lambda \approx 1.2$,¹⁷⁻¹⁹ to a strongly field-dependent γ_λ increasing with field and attaining a value of ~ 3.5 at a modest field of 5 kOe.^{16,20} Measurements of the electronic specific heat in MgB₂, which mainly reflects γ_ξ , yields an anisotropy which increases with the applied field.²¹

In this paper we will demonstrate a use of small-angle neutron scattering (SANS) to determine the penetration depth anisotropy in MgB₂, by measuring the misalignment between the applied field, \mathcal{H} , and the direction of the vortices in the FLL as the field is rotated between the *c* axis and the basal plane. Using a two-band/two-gap model we can fit the angular dependence of the misalignment. At 4.9 K and 4 kOe we find $\gamma_\lambda = 1.1 \pm 0.2$, smaller than SANS measurements of the FLL anisotropy in single crystals²⁰ and torque magnetometry,¹⁶ but in good agreement with SANS results on powders¹⁷ and scanning tunneling spectroscopy results.¹⁸

The misalignment corresponds to vortices canting towards the crystalline *c* axis.

The experiments were performed at the NG3 SANS instrument at the National Institute of Standards and Technology Center for Neutron Research. The sample was a ~ 200 μg platelike single crystal with the *c* axis parallel to the thin direction, grown using isotopically enriched ¹¹B to reduce neutron absorption.²² The ¹¹B concentration in the sample is estimated to be $\sim 95\%$, with $\sim 5\%$ ¹⁰B due to the use of a natural boron BN crucible (20% ¹⁰B, 80% ¹¹B) in the crystal growth. Incident neutrons with a wavelength $\lambda_n = 1$ nm and a wavelength spread $\Delta\lambda_n / \lambda_n = 14\%$ were used, and the FLL diffraction pattern was collected by a 650 mm \times 650 mm position sensitive detector with 5 mm resolution. Both the collimation and sample-to-detector distances were 8 m. All measurements were performed in a magnetic field of 4 kOe applied at different angles, $\theta = 0^\circ - 80^\circ$, with respect to the crystalline *c* axis. For all angles the field was rotated around the vertical crystalline [110] axis [see Fig. 1(a)], and the measurements were obtained following a field cooling procedure to a temperature of 4.9 K. The applied magnetic field is in the horizontal direction and approximately parallel to the direction of the incident neutron beam.

Figure 1 shows FLL diffraction patterns obtained for three different orientations of the applied field. Each image is a sum of the scattering from the FLL as the cryomagnet is rotated around the vertical axis in order to satisfy the Bragg condition for the different reflections. In Fig. 1(a) the field is applied parallel to both the sample *c* axis ($\theta = 0^\circ$) as well as the direction of the neutron beam. Consistent with our earlier reports, a hexagonal FLL is observed, with the lattice plane normals (Bragg peaks) along the *a* axis.²⁰ Applying the field at an angle with respect to the *c* axis leads to a distortion of the hexagonal FLL as shown in Fig. 1(b), and eventually a reorientation shown in Fig. 1(c). In contrast to $\mathcal{H} \parallel \mathbf{c}$ where the reorientation progresses continuously above an onset field $H^* \sim 5$ kOe,²⁰ the transition in rotated fields is first order and occurs at $\theta \sim 70^\circ$ with an applied field of 4 kOe. The FLL reorientation is attributed to the multigap nature of the superconductivity in this material.^{20,23} Previously the FLL anisotropy has been used as a measure of γ_λ .^{18,20} However, recent measurements have indicated that in MgB₂ in the proximity of the reorientation transition this anisotropy may

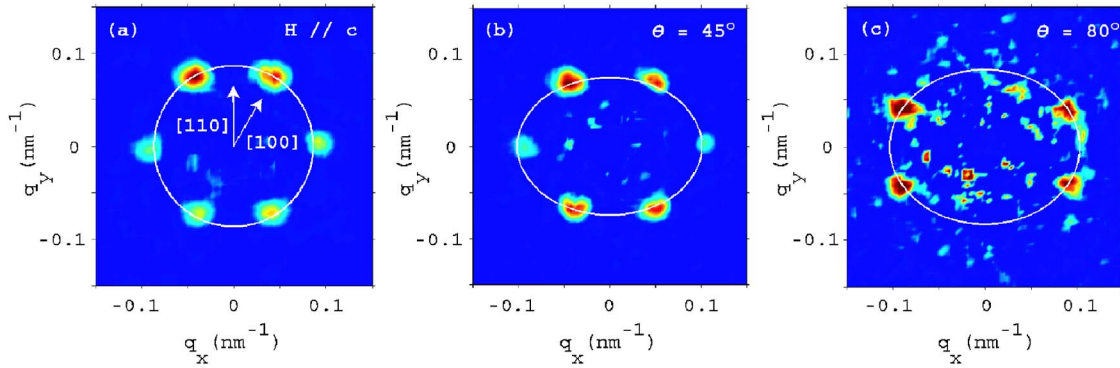


FIG. 1. (Color online) FLL diffraction patterns for MgB₂ obtained at 4 kOe and 4.9 K, and with the applied field at angles $\theta=0^\circ$ (a), 45° (b), and 80° (c) with respect to the c axis. The orientation of the sample crystallographic axes is shown in panel (a). The reflections on the vertical axis in panel (c) are absent since they do not satisfy the Bragg condition. The data are smoothed by a 5×5 box average.

be influenced by vortex core effects,²⁴ similar to what is observed in members of the borocarbide superconductors.²⁵ In contrast to the FLL anisotropy, the direction of the vortices in the FLL does not depend on vortex-vortex interactions in the plane perpendicular to the flux lines. Hence, measurements of the misalignment of the FLL with respect to the applied field provide a method for determining γ_λ , which is not affected by vortex core effects.

The exact orientation of the applied magnetic field is obtained from the FLL rocking curve with $\mathcal{H} \parallel c$. In this case the vortices are parallel to the applied field. In Fig. 2(a) the intensities of the Bragg peaks lying on the horizontal axis are plotted as a function of the cryomagnet rotation angle, α . The calibrated zero ($\alpha=0$) is determined from the position of the midpoint between the two peaks, obtained by Gaussian fits to the rocking curves. As the field is rotated away from the c axis the vortices in the FLL cant away from the direction of the applied field as shown in Figs. 2(b) and 2(c). The rocking curve midpoint now directly reflects the misalignment of the FLL, $\delta\theta$, with respect to the direction of the applied field. Note that above the FLL reorientation transition four Bragg peaks shown in Fig. 1(c) are centered around the horizontal axis and used to determine $\delta\theta$. The misalignment corresponds to the vortices being rotated towards the crystalline c axis. Only a slight increase in the average rocking curve width from $0.45^\circ \pm 0.05^\circ$ full width at half maximum (FWHM) ($\theta=0^\circ$) to $0.55^\circ \pm 0.05^\circ$ FWHM ($\theta=80^\circ$) is observed as the field is rotated away from the c axis, indicating that no significant disordering of the FLL takes place. The experimental resolution is estimated to be $\sim 0.25^\circ$ FWHM. The absolute scattered intensity from the FLL decreases due to the increased absorption, as the effective sample thickness becomes larger.

The results of the SANS measurements are summarized in Fig. 3. This shows a symmetrical $\delta\theta$ vs θ dependence, with a maximum $\delta\theta \approx 1^\circ$ close to $\theta=45^\circ$, and decreasing towards zero for $\theta=90^\circ$ as expected. Measurements at angles above 80° were not possible due to absorption and increasing background scattering from sample defects.

While the torque in a single-band superconductor is proportional to the misalignment, $\delta\theta$, this is not the case in materials with $\gamma_\lambda \neq \gamma_H$ such as MgB₂. In the following it is assumed that the sample can be approximated by an oblate

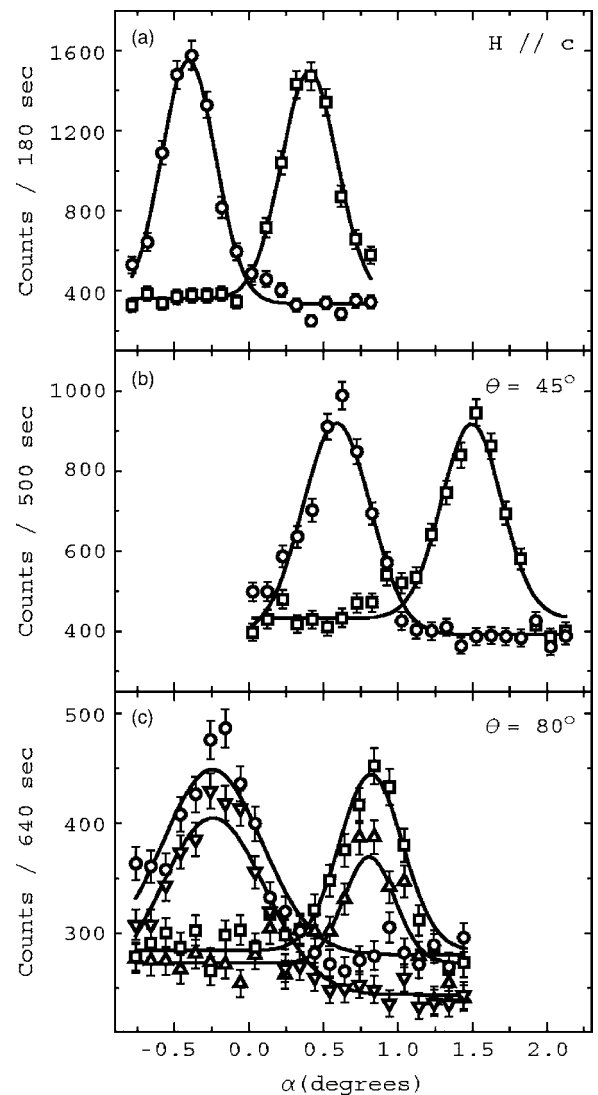


FIG. 2. FLL rocking curves for MgB₂ with the applied field at $\theta=0^\circ$ (a), 45° (b), and 80° (c) with respect to the c axis. The intensities at each angular setting, α , are obtained by summing the detector counts at the position of the Bragg reflections. The curves are Gaussian fits to the data. No background subtraction is performed.

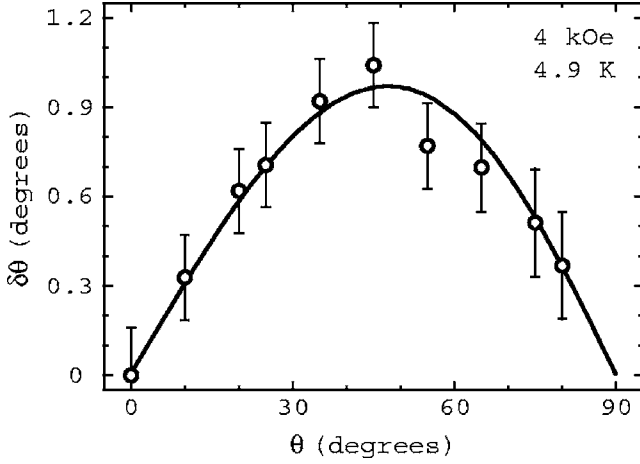


FIG. 3. FLL misalignment ($\delta\theta$) as a function of the applied field rotation (θ). The error bars take into account both the statistical and systematic errors of the measurements. The solid line is a fit to the data described in the text.

spheroid (a coin) with the c axis along z , and choosing (x, y) so that the applied field \mathcal{H} lies in the xz plane forming an angle θ with z . The linear relation between the applied field \mathcal{H} , the induction \mathbf{B} , and the magnetization \mathbf{M} reads²⁶

$$B_i = \mathcal{H}_i + 4\pi M_i(1 - n_i), \quad i = x, z, \quad (1)$$

where $n_z = 1 - 2n$ and $n_x = n$ are the demagnetization coefficients. For a coin-shaped sample $n \ll 1$. The angle, $\theta_B = \theta - \delta\theta$, between the induction and the c axis is given by

$$\tan \theta_B = \frac{B_x}{B_z} = \frac{\mathcal{H}_x + 4\pi M_x(1 - n_x)}{\mathcal{H}_z + 4\pi M_z(1 - n_z)}. \quad (2)$$

For $\mathcal{H} \gg H_{c1}$ where $M \ll \mathcal{H}$, as is the case in the present experiment, the misalignment $\delta\theta = \theta - \theta_B$ is thus given by

$$\frac{\delta\theta}{2\pi} = \sin 2\theta \left[\frac{M_z}{\mathcal{H}_z} 2n - \frac{M_x}{\mathcal{H}_x} (1 - n) \right]. \quad (3)$$

For materials with $\gamma_\lambda \neq \gamma_H$ the free energy density is given by⁶

$$\tilde{F} = F - \frac{B^2}{8\pi} = \frac{\phi_0 B \varepsilon_\lambda}{32\pi^2 \lambda^2 \gamma_\lambda^{1/3}} \ln \frac{4\eta H_{c2,c} \gamma_\lambda e}{B \varepsilon_\lambda (1 + \beta)^2}, \quad (4)$$

where $\lambda = (\lambda_{ab}^2 \lambda_c)^{1/3}$ is the average penetration depth, $\varepsilon_{\lambda,H}^2 = \sin^2 \theta_B + \gamma_{\lambda,H}^2 \cos^2 \theta_B$, and

$$\beta = \frac{\gamma_\lambda}{\gamma_H} \sqrt{\frac{B_x^2 + \gamma_H^2 B_z^2}{B_x^2 + \gamma_\lambda^2 B_z^2}} = \frac{\gamma_\lambda \varepsilon_H}{\gamma_H \varepsilon_\lambda}. \quad (5)$$

The constant η lumps together the London uncertainty factor ≈ 1.4 with $\pi\sqrt{3}/e$ yielding $\eta \approx 2.8$.

Evaluation of the magnetization, $\mathbf{M} = -\partial\tilde{F}/\partial\mathbf{B}$, and the misalignment angle, $\delta\theta$, is now straightforward. Differentiating with respect to (B_x, B_z) , and noting that $B \varepsilon_\lambda = \sqrt{B_x^2 + \gamma_\lambda^2 B_z^2}$, one obtains \mathbf{M} in terms of \mathbf{B}

$$\frac{M_x}{M_0} = -\frac{B_x \gamma_\lambda^{-1/3}}{B \varepsilon_\lambda} \left\{ \ln \frac{4\eta H_{c2,c} \gamma_\lambda}{(1 + \beta)^2 B \varepsilon_\lambda} + \frac{2\gamma_\lambda (\gamma_H^2 - \gamma_\lambda^2) \cos^2 \theta}{\gamma_H (1 + \beta) \varepsilon_\lambda \varepsilon_H} \right\}, \quad (6)$$

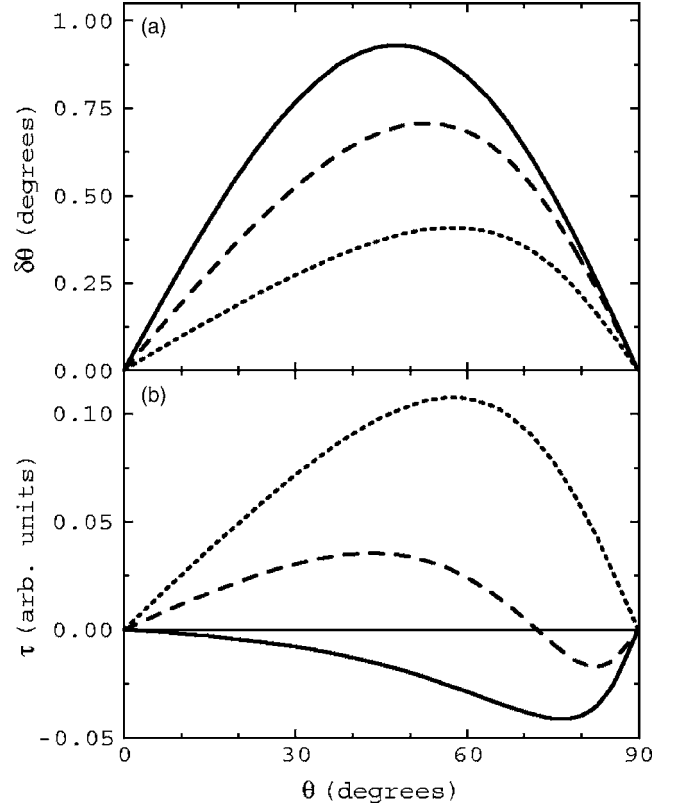


FIG. 4. Calculated misalignment (a) and torque (b) as a function of rotation angle, using Eqs. (8) and (9) with $\mathcal{H} = 4$ kOe, $\lambda = 155$ nm and $n = 0.01$. The curves correspond to low ($\gamma_H = 6$, $\gamma_\lambda = 1.1$, solid line), intermediate ($\gamma_H = 5.5$, $\gamma_\lambda = 1.5$, dashed line) and high ($\gamma_H = \gamma_\lambda = 2$, dotted line) temperatures.⁷

$$\frac{M_z}{M_0} = -\frac{B_z \gamma_\lambda^{5/3}}{B \varepsilon_\lambda} \left\{ \ln \frac{4\eta H_{c2,c} \gamma_\lambda}{(1 + \beta)^2 B \varepsilon_\lambda} - \frac{2(\gamma_H^2 - \gamma_\lambda^2) \sin^2 \theta}{\gamma_\lambda \gamma_H (1 + \beta) \varepsilon_\lambda \varepsilon_H} \right\}, \quad (7)$$

where $M_0 = \phi_0 / 32\pi^2 \lambda^2$. Since $M \ll \mathcal{H}$, the angle $\delta\theta$ is small and M_i 's in Eq. (3) can be taken in the lowest approximation. Substituting Eqs. (6) and (7) into Eq. (3) one can replace (B, θ_B) with (\mathcal{H}, θ) obtaining

$$\frac{\delta\theta}{2\pi} = \frac{M_0 \sin 2\theta}{\mathcal{H} \gamma_\lambda^{1/3} \varepsilon_\lambda} \left\{ (1 - n - 2n\gamma_\lambda^2) \ln \frac{4\eta H_{c2,c} \gamma_\lambda}{(1 + \beta)^2 \mathcal{H} \varepsilon_\lambda} + \frac{2\gamma_\lambda (\gamma_H^2 - \gamma_\lambda^2)}{\gamma_H (1 + \beta) \varepsilon_\lambda \varepsilon_H} [(1 - n) \cos^2 \theta + 2n \sin^2 \theta] \right\}. \quad (8)$$

For MgB_2 , $\gamma_H > \gamma_\lambda$ at all temperatures, and hence $\delta\theta > 0$ for all values of θ and T provided that n is small. Consequently, for a coin-shaped sample, the vortices are expected to rotate towards the c axis, consistent with the experimental results.

The solid line in Fig. 3 is the best fit of Eq. (8) to the SANS data, obtained by varying γ_λ and λ , while setting $\gamma_H = 6$, $\eta = 2.8$ and using an approximate demagnetization factor for the sample, $n = 0.01$. This yields a value $\gamma_\lambda = 1.1 \pm 0.2$ and $\lambda = 155$ nm. The results provide additional evidence for a low value of γ_λ even at this relatively high field. Due to the uncertainty on the parameter η as well as the demagnetization factor, n , a reliable determination of λ and γ_H is difficult, especially since changing these two param-

eters both affects only the amplitude of $\delta\theta$. Nonetheless, the fitted value of λ is within the range of literature values summarized in Ref. 8 and in fair agreement with $\lambda=136$ nm from Ref. 16. However, we cannot exclude a field dependent $\gamma_\xi(H)$ merging with γ_H at H_{c2} , as suggested in Refs. 14, 16, and 21. On the other hand, the profile of $\delta\theta$ is determined solely by γ_λ , allowing a reliable fit of this parameter. Increasing γ_λ causes the $\delta\theta$ profile to become more asymmetric, as shown in Fig. 4(a). Although it would be possible to fit our data with $\gamma_H=\gamma_\lambda=1.1$ and $\lambda=135$ nm, this is an unreasonably low value of γ_H for a field of 4 kOe, and consequently the results presented here do not support a single anisotropy factor as proposed in Refs. 14 and 16.

Finally, it is of interest to compare $\delta\theta$ to the torque density, $\tau_y=M_c\mathcal{H}_x-M_x\mathcal{H}_z$. Inserting the M_i 's from Eqs. (6) and (7) one obtains⁶

$$\tau_y = \frac{M_0\mathcal{H} \sin 2\theta}{2\gamma_\lambda^{1/3}\epsilon_\lambda} \left\{ (\gamma_\lambda^2 - 1) \ln \left(\frac{4\eta H_{c2,c}\gamma_\lambda}{(1+\beta)^2\mathcal{H}\epsilon_\lambda} \right) - \frac{2\gamma_\lambda(\gamma_H^2 - \gamma_\lambda^2)}{\gamma_H(1+\beta)\epsilon_\lambda\epsilon_H} \right\}. \quad (9)$$

Comparing this to Eq. (8) it is clear that in general $\delta\theta$ is not proportional to τ_y , as only the former is shape dependent. In

particular, Eq. (9) suggests that at low temperature the torque is negative as shown in Fig. 4(b), in contrast to what has been observed for layered superconductors.^{27,28} Near T_c one recovers $\delta\theta \propto \tau_y$, as in materials with $\gamma_\lambda = \gamma_H$. Given the success of the model presented here in describing the misalignment, it would be of interest to test further the relationship between $\delta\theta$ and the torque. Finally, one notes that for a spherical sample with $n=1/3$ one finds $\delta\theta \propto \tau_y$ for all values of γ_λ and γ_H .

In summary, we have shown that SANS measurements of the misalignment angle between the applied field and the FLL can provide information about the penetration depth anisotropy in MgB₂. At 4.9 K and 4 kOe we find a relatively low value of $\gamma_\lambda = 1.1 \pm 0.2$. More studies are needed to extend the measurements of γ_λ to both higher temperatures and fields, in order to investigate the entire mixed phase of MgB₂.

We are grateful to J. Barker and P. Butler for their help during the SANS experiment. We acknowledge the support of the National Institute of Standards and Technology, U.S. Department of Commerce, in providing the neutron research facilities used in this work. This work utilized facilities supported in part by the National Science Foundation under Agreement No. DMR-0454672.

*Electronic address: eskildsen@nd.edu

¹A comprehensive review can be found in *Physica C* **385** (2003), special issue, edited by W. Kwok, G. Crabtree, S. L. Bud'ko, and P. C. Canfield.
²J. Kortus *et al.*, *Phys. Rev. Lett.* **86**, 4656 (2001).
³A. Y. Liu, I. I. Mazin, and J. Kortus, *Phys. Rev. Lett.* **87**, 087005 (2001).
⁴H. J. Choi, D. Roundy, H. Sun, M. L. Cohen, and S. G. Louie, *Nature (London)* **418**, 758 (2002).
⁵V. G. Kogan, *Phys. Rev. B* **66**, 020509(R) (2002).
⁶V. G. Kogan, *Phys. Rev. Lett.* **89**, 237005 (2002).
⁷P. Miranović, K. Machida, and V. G. Kogan, *J. Phys. Soc. Jpn.* **72**, 221 (2003).
⁸A. A. Golubov, A. Brinkman, O. V. Dolgov, J. Kortus, and O. Jepsen, *Phys. Rev. B* **66**, 054524 (2002).
⁹F. Simon *et al.*, *Phys. Rev. Lett.* **87**, 047002 (2001).
¹⁰G. Papavassiliou, M. Pissas, M. Fardis, M. Karayanni, and C. Christides, *Phys. Rev. B* **65**, 012510 (2001).
¹¹M. Angst *et al.*, *Phys. Rev. Lett.* **88**, 167004 (2002).
¹²S. L. Bud'ko and P. C. Canfield, *Phys. Rev. B* **65**, 212501 (2002).
¹³M. Zehetmayer, M. Eisterer, J. Jun, S. M. Kazakov, J. Karpinski, A. Wisniewski, and H. W. Weber, *Phys. Rev. B* **66**, 052505 (2002).

¹⁴L. Lyard *et al.*, *Phys. Rev. Lett.* **92**, 057001 (2004).

¹⁵A. Rydh *et al.*, *Phys. Rev. B* **70**, 132503 (2004).

¹⁶M. Angst *et al.*, *Phys. Rev. B* **70**, 224513 (2004).

¹⁷R. Cubitt, S. Levett, S. L. Bud'ko, N. E. Anderson, and P. C. Canfield, *Phys. Rev. Lett.* **90**, 157002 (2003).

¹⁸M. R. Eskildsen *et al.*, *Phys. Rev. B* **68**, 100508(R) (2003).

¹⁹J. D. Fletcher, A. Carrington, O. J. Taylor, S. M. Kazakov, and J. Karpinski, *Phys. Rev. Lett.* **95**, 097005 (2005).

²⁰R. Cubitt, M. R. Eskildsen, C. D. Dewhurst, J. Jun, S. M. Kazakov, and J. Karpinski, *Phys. Rev. Lett.* **91**, 047002 (2003).

²¹F. Bouquet, Y. Wang, I. Sheikin, T. Plackowski, A. Junod, S. Lee, and S. Tajima, *Phys. Rev. Lett.* **89**, 257001 (2002).

²²J. Karpinski *et al.*, *Supercond. Sci. Technol.* **16**, 221 (2003).

²³M. E. Zhitomirsky and V.-H. Dao, *Phys. Rev. B* **69**, 054508 (2004).

²⁴R. Cubitt, M. R. Eskildsen, and C. D. Dewhurst (to be published).

²⁵M. R. Eskildsen *et al.*, *Phys. Rev. Lett.* **86**, 320 (2001).

²⁶L. D. Landau, E. M. Lifshitz, and L. P. Pitaevskiĭ, *Electrodynamics of Continuous Media*, 2nd ed. (Pergamon, Oxford, 1984), Sec. 29.

²⁷J. M. Tranquada *et al.*, *Phys. Rev. B* **37**, 519 (1988).

²⁸D. E. Farrell, C. M. Williams, S. A. Wolf, N. P. Bansal, and V. G. Kogan, *Phys. Rev. Lett.* **61**, 2805 (1988).